Lab on a Chip

PAPER

View Article Online
View Journal | View Issue

Cite this: *Lab Chip*, 2023, **23**, 3662

Tuning the hydraulic resistance by swelling-induced buckling of membranes in high-aspect-ratio microfluidic devices†

Claas-Hendrik Stamp, [ab] Binyam Solomon,[a] Friederike Lang,[a] Efstathios Mitropoulos[ab] and Thomas Pfohl *[ab]

Controlling fluid flow in microfluidic devices and adapting it to varying conditions by selectively regulating hydrodynamic properties is of critical importance, as the field of microfluidics faces increasingly complex challenges in its wide range of applications. One way to manipulate flows in microfluidic devices is to introduce elastic elements that can be actively or passively deformed. In this work, we developed a membrane-based microfluidic device that allows us to study the deformation of swollen thin membranes as a function of the volume fractions in binary mixtures – here isopropanol and water. Furthermore, the membrane deformation can be used to control pressure-driven flows within the device. The device consists of two microfluidic channels separated by a thin membrane that deforms by a buckling-based mechanism, when the isopropanol volume fraction of the solvent flowing through it exceeds a certain volume fraction. The buckling membrane causes a sinusoidal height variation in both adjacent channels, resulting in a large increase in hydraulic resistance. We show that buckling-based deflections of elastic membranes can be used to amplify small changes in the degree of swelling to produce large changes in the microchannel geometry of the device, sufficient to manipulate the flow rate of pressure-driven flows in the microdevice.

Received 5th December 2022,
Accepted 10th July 2023

DOI: 10.1039/d2lc01120d

rsc.li/loc

Introduction

Elastically deformable elements enable precisely defined conditions for controlling fluid flows in microfluidics for a wide variety of applications. Quake and coworkers used elastic elements as pneumatically activated valves to guide and control fluid flows in microfluidic networks.[1–3] The valves are based on thin channel walls, which can block the flow through a primary channel by inflating control channels.[2,3] In addition, they also were able to build micropumps based on this method.[3] The combination of (pneumatically) deformable membranes and electrostatic repulsion – "soft electrostatic trapping" – enables the trapping and release of particles within geometrical confinements.[4–6] This method allows the trapping of nano-objects in well-defined arrays and provides a reliable platform for the manipulation of them.

The aforementioned examples were mainly realized in microfluidic channel systems based on the elastomer polydimethylsiloxane (PDMS). The targeted deformations of the channel geometry and their cross-sectional areas drastically affect the effective pressure drop and the corresponding flow rates in pressure-driven flows.[7,8] Based on these properties, passive devices were developed that stabilize a pulsating incoming flow and generate a steady flow from the device. The flow stabilizer consists of several chambers, whose covers are flexible membranes that deflect as fluid flows through the system at oscillating flow rates. The in- and outward deflection of the membranes during an over- or underflow phase results in a change of volume in the chambers. The chambers act as reservoirs that stabilize flows by storing and releasing solvent, analogous to a capacitor in an electrical circuit.[9]

Another way to passively control pressure-driven flows is realized using a snap-through mechanism of an elastic element. In rectangular channels, one of the channel walls was replaced by a flexible polyethylene stripe, clamped at both ends forming an arch, bent into the channel, resulting in a constriction with increased hydraulic resistance. Exceeding a critical flow rate, the arc snaps trough and deflects out of the channel, increasing the cross-sectional area, which results in a lifting of the constriction and a reduction of the hydraulic resistance.[10] To use an arch to actively control pressure-driven flows, a flexible microfluidic device was fabricated in which a

[a] *Physikalisches Institut, Albert-Ludwigs-Universität Freiburg, Hermann-Herder-Straße 3, 79104 Freiburg, Germany. E-mail: thomas.pfohl@physik.uni-freiburg.de*
[b] *Cluster of Excellence livMatS, Albert-Ludwigs-Universität Freiburg, FIT – Freiburg Center for Interactive Materials and Bioinspired Technologies, Georges-Köhler-Allee 105, 79110 Freiburg, Germany*

† Electronic supplementary information (ESI) available. See DOI: https://doi.org/10.1039/d2lc01120d

wall of the microfluidic channel was replaced by an arch that bent into the channel. By applying a stress to the device, the height of the arch can be adjusted, resulting in direct control of the hydraulic resistance and corresponding flow rates of pressure-driven viscous flows.[11]

In addition to these passively or actively controlled devices, there is a need for adaptive elements that change their behavior as a response to a trigger, such as the change of solvent properties. For example, swelling of thin gel films under constraints is a possible route of designing 3D-patterns from 2D-templates.[12–14] Swelling of materials leads to internal stresses in the material, and out-of-plane deformations occur when a critical threshold is exceeded. Rectangular plates with one edge clamped show a periodic buckling pattern of a sinusoidal shape along the free edge.[15,16] For rectangular plates with two edges clamped along the long side, a similar buckling pattern is observed. The part of the membrane between the two clamped edges deforms along the long side with a sinusoidal buckling pattern, while the clamped edges maintain their straightness.[16] The buckling patterns of rectangular plates under various conditions are described in detail in the literature.[17–22] Depending on the boundary conditions, the shape of the plate and the load distribution along the plate, different pattern shapes can be obtained, and the conditions under which buckling occurs can be adjusted. There are also approaches to further manipulate generated buckling patterns by compressing or stretching to obtain more complex buckling patterns.[23] To predict the swelling of polymer gels, theoretical frameworks were developed, which allow for the explanation of the initial buckling, the buckling stress, and the initial shape of the buckling patterns.[24,25] However, except for a few closed-form solutions in simple cases, there are no analytical solutions for more complex shapes, and most of the behavior must be predicted by numerical solutions.[15,16,26,27]

The buckling mechanism allows us to change the geometry of microfluidic channels as a function of the swelling of the device material used, offering a potential approach to manipulate pressure-driven viscous flows in microfluidic devices. In this paper, we present a buckling-based hydraulic resistor that abruptly changes the flow rate of pressure-driven flows through the device when the isopropanol volume fraction ϕ_{iso} of a binary mixture of isopropanol and water exceeds the volume fraction of observed buckling, ϕ_b.

Experimental

Fabrication of microfluidic devices

We designed microfluidic devices consisting of two adjacent channels, separated by a thin membrane. The membrane has a length a = 1000 μm, width b = 200 μm, and height h_m = 20 μm (Fig. 1). The flow channels running on both sides of the membrane (Fig. 1a and b) have the same dimensions, their length is a = 1000 μm, their width b = 200 μm, and their

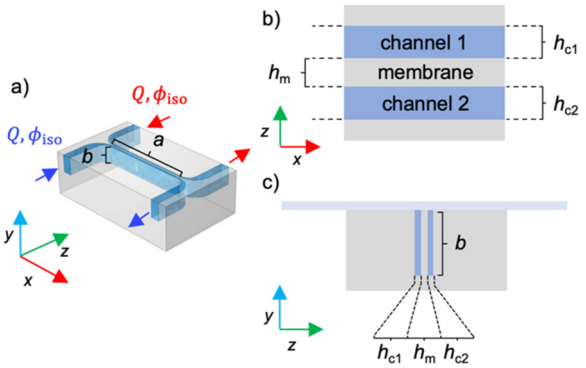

Fig. 1 a) Pseudo 3D-view of a section of the microfluidic device. The channels are shown in blue and can be flushed with binary mixtures with an isopropanol volume fractions ϕ_{iso} and volume flow rates of Q. The membrane has a length a and a width b. b) Schematic side view (xz-plane) of the microfluidic device with a membrane (grey) between the two channels (blue), whose outer sides are defined by the channel walls (grey). The membrane height is h_m and the channels heights are $h_{c1} = h_{c2}$. c) Side view of the device on the yz-plane. One side of the microfluidic device is covered with a microscope slide (light blue) which is the channel ceiling of one side of the microfluidic channels.

height $h_{c1} = h_{c2}$ = 20 μm. The height of the connecting channels before and after the membrane segment is 100 μm, whereas the width of all device structures is b = 200 μm. One side of the membrane is covalently bonded to a microscope slide, which covers the whole device while the other sides are connected to PDMS (Fig. 1c).

The devices were fabricated by soft lithographic replica molding.[28] The master used for the microfabrication process is based on SU8 photoresist and fabricated by Microresist, Berlin, Germany, using a 5″-chrome photomask (Compugraphics, Jena, Germany) for UV-lithography. To prevent covalent binding during the soft lithography process, the master was hydrophobized with chloro-trimethyl-silane vapor (≥99%, Sigma Aldrich, Burlington, MA., USA). To build the device, we used Sylgard Elastomer Kit 184 (Dow Inc., Midland, MI., USA). The PDMS from the kit was mixed with the curing agent in a ratio of 10 : 1 by vigorous stirring, and air bubbles were removed in a subsequent degassing step at a pressure below 2 mbar. Then the PDMS was poured over the master. To ensure complete coverage of the microstructure of the master, air bubbles trapped in small gaps of the master were removed in an additional degassing step performed at a pressure of below 2 mbar. The curing was carried out overnight at a temperature of 65 °C. The connection holes for the solvents in- and outlet tubing were punched into the PDMS replica using a disposable biopsy punch with a diameter of 1 mm (Kai Industries Co. Ltd. Oyana, Japan). Prior to binding, excess non-crosslinked PDMS oligomers were removed by washing the device in chloroform (pa., Merck, Darmstadt, Germany) three times for 24 h. After the washing step, the device was placed in a desiccator and the pressure was set to 2 mbar in order to remove all residues of the chloroform. The drying step additionally serves to straighten the membrane, which may

collapses during cutting and punching (ESI† S1). From the drying step on onwards, the device must be handled with special care to prevent the membrane from collapsing. To prepare the microscope slide (1 mm × 76 mm × 26 mm, R. Langenbrinck GmbH, Emmendingen, Germany) for the binding process, the slide was cleaned in isopropanol (IR grade, Carl Roth, Karlsruhe, Germany) in a Sonorex ultrasonic bath (Bandelin, Berlin, Germany). After cleaning, the slide was dried under nitrogen flow and was activated together with the PDMS replica in a Zepto plasma cleaner (Diener, Ebhausen, Germany) in ambient atmosphere at a pressure of <10 mbar. After activation, the PDMS replica was placed on the microscope slide and the covalent binding was enhanced by heating the microfluidic device on an IKAMAG RCT heat plate (IKA, Staufen, Germany) at around 100 °C for 15 min. After binding, the membrane is checked for proper connection to the microscope slide (ESI† S2). The device was connected to solvent reservoirs by Teflon tubes of an inner diameter of 0.40 mm (Reichelt Chemietechnik, Heidelberg, Germany).

Imaging

The micrographs were taken with an Olympus BX61 (Olympus, Hamburg, Germany), equipped with an Olympus LMPlan FI 10×/0.25 objective and an Imagesource (Bremen, Germany) DMK 33UX174 Camera. The contrast and brightness of the micrographs were adjusted using Fiji.[29] The focal plane of all micrographs was set to $1/2b$ using a MP – 285 *xyz*-stage (Sutter Instrument Company, Novato, CA, USA) to position the microfluidic device under the microscope.

Buckling membranes

For the investigations, binary mixtures of isopropanol (IR grade, Carl Roth, Karlsruhe, Germany) and water with volume fractions from ϕ_{iso} = 0.000 to ϕ_{iso} = 1.000 were flushed through the device. Solvents were exchanged by forcing them through the channels and replacing most of them with air using a 1 ml syringe filled with air (Braun, Bethlehem, PA, USA). After solvent exchange, the membrane was 'equilibrated' for at least 1 hour at a volumetric solvent flow rate of $Q > 1$ μl s^{-1} using a Nemesys syringe pump (Cetoni, Korbussen, Germany) and a 1 ml syringe. The washing period prevents possible fluctuations in ϕ_{iso} caused by residual solvents in the channels and effusing solvents from the PDMS bulk material into the channels. There was no fluid flow through the channels, during the imaging process. Between measurements of the binary mixtures with different ϕ_{iso}, the buckling pattern was made to disappear by flushing the solvent mixture with $Q > 10$ μl s^{-1}. Setting Q = 0 μl s^{-1}, the deflection-pattern formed again and images of the pattern were acquired. The procedure was carried out ten times.

The wavelength λ of the membrane deformations ('buckles') was measured by integrating the intensity of the membrane deformations perpendicular to the initial position of the membrane in the micrographs and normalizing the resulting intensity profiles to the number of pixels over which they were integrated. The average intensity profile of each micrograph was fitted with Gaussian functions using the numeric computing environment Matlab (MathWorks, Aachen, Germany) from which the individual buckle positions were obtained (ESI† S3). By calculating the length of the individual buckles, the average $1/2\lambda$ were obtained.

r_{max} is the maximum displacement of the membrane relative to its initial position in the center of the channel system. For isopropanol volume fractions below the fraction at which buckling is observable ($\phi_{iso} < \phi_b$), the membrane displacement was measured at $y = 1/2b$ and x = 100, 300, 500, 700 and 900 μm. For $\phi_{iso} > \phi_b$ the position of the membrane was measured at $y = 1/2b$ and at the position of maximum deflection for each buckle. The measurements for each ϕ_{iso} were made on five different shapes obtained by rapidly flushing the channel system, which caused the instability to disappear; subsequently the flow rate was set to zero, allowing the membrane to reach its 'equilibrium position' of the corresponding concentration. The amount of difference between the individual membrane positions and their initial position in the center of the channel was averaged for the different ϕ_{iso}, resulting in r_{max}. The position vectors were determined from the micrographs by using Fiji image processing software.[29]

Hydraulic resistance

For the measurements of the hydraulic resistance inside the devices, binary isopropanol–water mixtures of different volume fractions (ϕ_{iso} = 0.000 to 1.000) were flown through the device by applying a hydrostatic pressure difference (Δp) between the in- and the outlet. To set Δp, we used two syringes without pistons, which were used as solvent reservoirs and connected *via* tubing to the device. By changing the relative height Δl between the device outlet and the solvent surfaces in the syringes, we set the pressure difference Δp between the in- and outlet, which was calculated by $\Delta p = \rho g \Delta h$, with the density ρ, the acceleration due to gravity g and the height difference between the inlet and the outlet of the microfluidic device Δh. The local flow fields were determined by particle imaging velocimetry (PIV), using fluorescently labeled colloidal polystyrene-based particles (Sigma Aldrich, Burlington, MA., USA) with a diameter of d = 1.0 μm for tracking. The flow fields V were measured approximately 200 μm upstream of the membrane section, where the channel height is 100 μm, with PIVLab[30] using ensemble averaging of 500 frames, setting the focal plane at $1/2b$. The flow rates were determined in good approximation from the product of the cross-section A and the average velocity v by $Q \approx Q^* = 2/3 \cdot v_{max} \cdot A$. v is calculated under the assumption of laminar flow from the maximum velocity in the middle of the channel $v = 2/3 v_{max}$ (ESI† S4). The hydraulic resistance $R(\phi_{iso})$ was obtained by fitting the initial slope of the Q^* *vs.* Δp plots, which is defined as the

inverse of the slope. To obtain the corrected hydrodynamic resistance, $R^*(\phi_{iso})$ was rescaled to the initial channel width $h_{c,\phi=0}$ at $\phi_{iso} = 0$ (ESI† S5).

Swelling ratio

The swelling ratio γ is defined as the ratio of the length of a PDMS object in the swollen state l and the length of the object in the dry state l_0 ($\gamma = l/l_0$). To measure γ, PDMS cubes with an edge length of roughly 5 mm with a pattern of position markers (pillars of 200 μm in height and with a length of around 100 μm, ESI† S6) at the top side were used. The cubes were cut from the mold that makes up the PDMS device and were washed and dried like the device. Before and after swelling in binary mixtures of different ϕ_{iso}, micrographs of the PDMS cubes were taken. Around 30 positions of the pillars were determined from the micrographs using Fiji.[29] Comparing the positions in dry and swollen states leads to an average γ of more than 500 individual γ_i. The swollen state was measured after a swelling period of 24 h.

Results and discussion

Swelling and buckling of microfluidic PDMS membranes by binary mixtures of isopropanol and water

Thin membranes of high aspect ratios can undergo swelling-induced buckling transitions and thus change their shape from 2D to 3D, when the swelling ratio of buckling γ_b is overcome.[15,16,25] These shape transitions may be used to manipulate pressure-driven flows that come in contact with these membranes. In order to study the interactions between fluids and elastic membranes including possible buckling states, we designed microfluidic devices in which a thin membrane of a high aspect ratio ($b/h_m = 10$) is embedded between two channels (Fig. 1). In our studies, the membranes had a length a = 1000 μm, width b = 200 μm and height h_m = 20 μm, the two adjacent channels had the dimensions of a = 1000 μm, b = 200 μm and channel heights $h_{c1/2}$ = 20 μm. The membrane is fixed at their edges, preventing lateral movement, but it is free to undergo out-of-plane deformations, limited only by its elastic properties. In our experiments, we observed and analyzed how the membrane behaves when exposed to binary isopropanol–water mixtures of different isopropanol volume fractions from ϕ_{iso} = 0.000 to 1.000.

Side views of exemplary membranes exposed to binary mixtures of different isopropanol volume fractions ϕ_{iso} are shown in Fig. 2. When the channels were filled with pure water, ϕ_{iso} = 0.000, the membrane had a rectilinear shape (Fig. 2a). The membrane and the corresponding channel walls appear slightly brighter than the adjacent water-filled channels. The contact surfaces of the channel walls with the binary mixture were aligned parallel to the line of sight of the microscope, causing them to appear as thin, faint lines on the micrographs. Filling the channels with isopropanol–water mixtures of ϕ_{iso} = 0.972 results in periodic deflections of the membrane (Fig. 2b). The membrane bent in a sinusoidal out-of-plane deflection into the adjacent channels 1 and 2, which resulted in a buckling membrane being framed by the two channel walls. If ϕ_{iso} was increased even further to pure isopropanol, ϕ_{iso} = 1.000, more pronounced buckling patterns of the membrane were observed, leading to a decrease in the wavelength of the deflection pattern (Fig. 2c). Moreover, the buckling membrane partially touched the limiting channel walls under additional slight deformations due to contact with the walls.

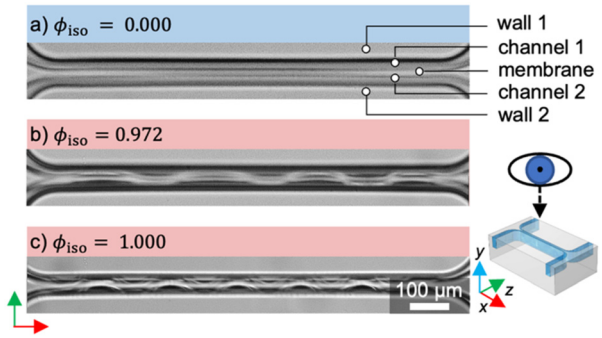

Fig. 2 Side view of the membrane in microfluidic device exposed to binary mixtures of different ϕ_{iso}. The focal plane of the micrographs was set at 1/2b of the membrane (not-buckling ■, buckling ■). Right-hand side: Labeling of the parts of the device and schematic pseudo-3D view on the device describing the line of sight to the device. a) ϕ_{iso} = 0.000. The membrane had a straight shape. b) ϕ_{iso} = 0.972. The membrane was buckling, but did not touch the walls. c) ϕ_{iso} = 1.000. The membrane was buckling and partially touched the walls.

The observed periodic out-of-plane deflections $w_{n,m}$ for $\phi_{iso} \geq 0.972$ depend on the numbers of buckles in x- and y-direction, n and m, the length a, width b, and the maximum deflection w_{max} (Fig. 3). $w_{n,m}$ can be described by:[17]

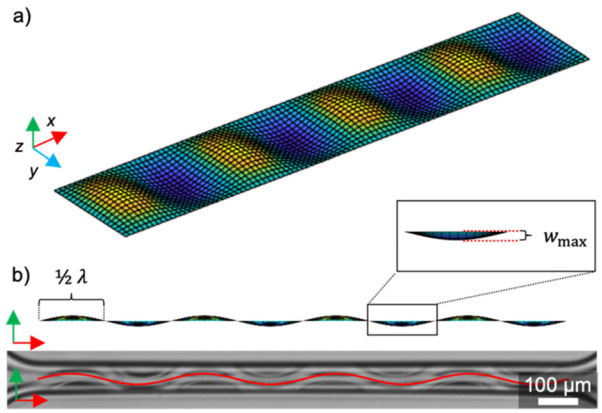

Fig. 3 Deflection pattern of a membrane of a = 1000 μm, b = 200 μm, h_m = 20 μm with w_{max} = 10.1 μm, n = 8, and m = 1 (parameters correspond to experiments with ϕ_{iso} = 0.976) a) Pseudo 3D view of the calculated deflection pattern. b) Top: Side view of the calculated deflection pattern with marking of 1/2λ and a zoom in with marking of w_{max}. Bottom: Micrograph of a membrane exposed to a mixture of ϕ_{iso} = 0.976 with the deflection pattern of the neutral plane at y = 1/2b (red).

$$w_{n,m} = w_{\max} \sin\left(\frac{nx\pi}{a}\right) \sin\left(\frac{my\pi}{b}\right). \quad (1)$$

For a detailed analysis of the observed buckling patterns, we determined $w_{n,m}$, the number n of the buckles in the x-direction, whereas m = 1 for the number of buckles in y-direction of all observed buckling membranes (ESI† S7), and the average wavelength of out-of-plane deformations λ. As an example, a pseudo 3D view of a deflecting surface is shown in Fig. 3a. The surface deflections are calculated for ϕ_{iso} = 0.976 using the measured parameters n, m, and w_{max}, which is equal to the maximum displacement of the membrane from its initial position in the middle of the channel r_{max}, for buckled membranes (periodic buckling patterns: $w_{max} \equiv r_{max}$). By superimposing the deflection surface with $y = 1/2b$ on the micrograph, it becomes apparent that the shape of the membrane and the calculated deflection surface are in good agreement. For $x \to 0$ and $x \to a$, discrepancies occur between the actual shape of the membrane and the calculated deflection surface due to the boundary conditions at the edge of the membrane (Fig. 3b, bottom). A side view of the calculated deflected surface with specified $1/2\lambda$ and w_{max} is shown in Fig. 3b (top).

The maximum displacement of the membrane r_{max} as a function of ϕ_{iso}, spanning the whole range from ϕ_{iso} = 0.000 to ϕ_{iso} = 1.000, is shown in Fig. 4a. The response of the membrane to mixtures with different ϕ_{iso} can be divided into two regimes, classified by different shapes of the membrane: the regime of non-buckling, and the regime of buckling.

In the non-buckling regime, no out-of-plane deformations from the neutral plane of the membranes are observed and $w_{max} \equiv 0$. This regime spans from ϕ_{iso} = 0.000 to ϕ_{iso} = 0.960. At ϕ_{iso} = 0.968, the membrane starts to deflect from its initial position ($r_{max} > 0$), this point is defined as the point of buckling, with the volume fraction of observed buckling, ϕ_b, and shows small out-of-plane deformations, but no periodic buckling patterns which can be described by eqn (1) (ESI† S8). At ϕ_{iso} = 0.972, ϕ_b is exceeded, and the membranes undergo out-of-plane deformations with periodic buckling patterns and $w_{max} \equiv r_{max}$. This transition can be identified by an increase of r_{max} if $\phi_{iso} > \phi_b$ (Fig. 4a) and the occurrence of periodic buckling with a defined number of buckles n (Fig. 4b, top) and half wavelength $1/2\lambda$ (Fig. 4b, bottom). By a further increase of ϕ_{iso}, the maximum deflection of the deformed membrane increases until r_{max} reaches a maximal value of r_{max} = (13.6 ± 1.0) μm at ϕ_{iso} = 0.984. From ϕ_{iso} = 0.000 to ϕ_{iso} = 0.984 the deformed membrane does not touch the channel walls. At $\phi_{iso} > 0.984$, the buckling membranes are partially touching the channel walls, r_{max} cannot further increase due to the direct contact with the channel walls.

In the range from ϕ_{iso} = 0.972 to 1.000, the membranes deflect with well-defined buckling patterns, which can be described by eqn (1). The number of buckles n at different ϕ_{iso} was measured ten times per ϕ_{iso}, with the most frequent n occurring at least with a frequency of 8/10. n depending on

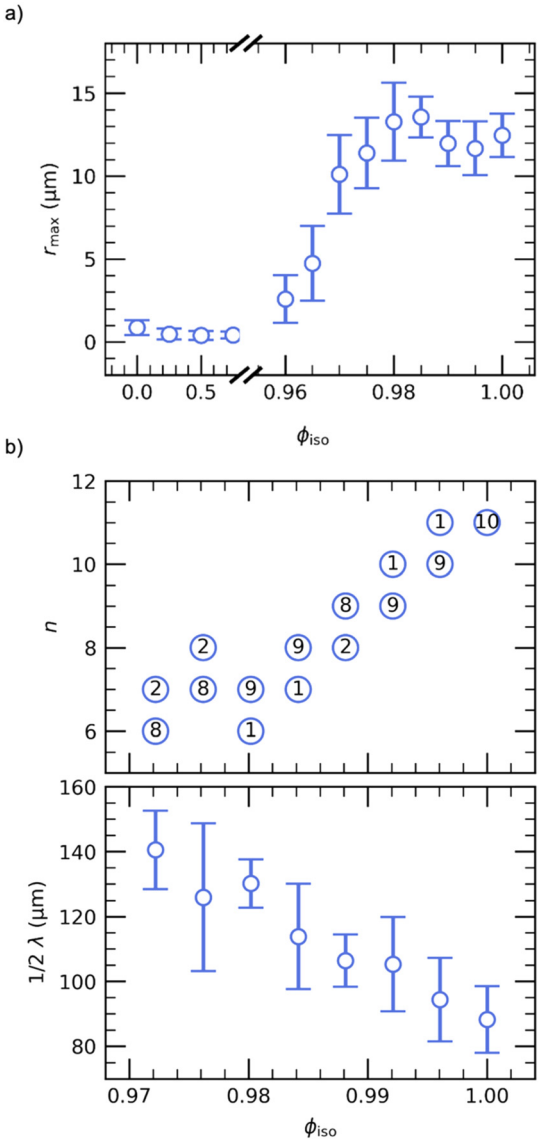

Fig. 4 a) Maximum deflection r_{max} of PDMS membranes exposed to binary isopropanol–water mixtures of ϕ_{iso}. b) Top: Number of buckles n and their frequency of appearance in a series of 10 experiments (integer inside the marker), formed by exposing the membrane to different ϕ_{iso}. Bottom: Half wavelength $1/2\lambda$ of the buckling patterns formed by exposing the membrane to different ϕ_{iso}.

ϕ_{iso} with its relative frequency is shown in Fig. 4b (top). The membrane deflects over its whole length a, causing a decrease of $1/2\lambda$ while n increases with ϕ_{iso} (Fig. 4b, bottom). $1/2\lambda$ ranges from (141 ± 12) μm at ϕ_{iso} = 0.972 with a most frequent n = 6 to (88 ± 10) μm at ϕ_{iso} = 1.000 with a most frequent n = 11. In the non-buckling regime neither n nor $1/2\lambda$ can be measured.

The described buckling of membranes in contact with binary isopropanol–water mixtures is driven by the swelling of PDMS and is therefore depending on ϕ_{iso}. The degree of swelling is characterized by the swelling ratio $\gamma = l/l_0$, where l is the length of a PDMS object in solvent and l_0 is the length of the dry PDMS object. A strong non-linear dependency of γ

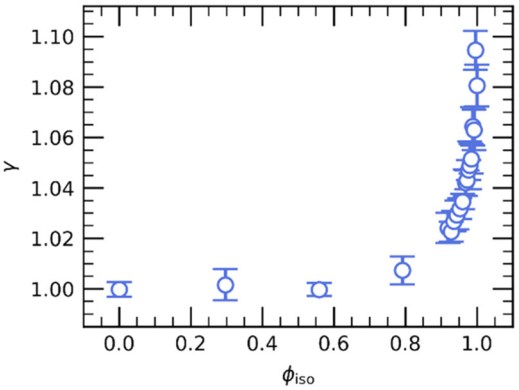

Fig. 5 Degree of swelling γ of PDMS caused by immersing it in binary isopropanol–water mixtures of different ϕ_{iso}.

on ϕ_{iso} can be found (Fig. 5). At $\phi_{iso} \lesssim 0.8$, almost no swelling is observed and regardless of ϕ_{iso} γ remains almost constant. Above this value, PDMS swells with increasing ϕ_{iso} to a maximum value of $\gamma \approx 1.09$.

When a straight, not buckled membrane comes into contact with binary isopropanol–water mixtures, the PDMS of which the membrane is made of swells depending on ϕ_{iso}. When $\gamma > 1$, the membrane increases its volume. The boundary conditions of the membrane at its edges prevent lateral movement, but allow out-of-plane deformations. Because of the boundary conditions, a lateral stress rises along the xy-plane. The lateral stress inside the membrane can be described with its Young's modulus E and its Poisson's ratio ν by:[31]

$$\sigma = \frac{E(\gamma - 1)}{1 - \nu}, \tag{2}$$

under the assumption of isotropy, with $E = E_x = E_y$, $\gamma = \gamma_x = \gamma_y$, and $\nu = \nu_{xy} = \nu_{yx}$. As γ increases, σ increases, and at the buckling point, the bending stiffness of the membrane is lower than the stretching stiffness, resulting in energy minimization by buckling the membrane;[16–18,32] analogously, λ, n, and w_{max} change with ϕ_{iso} (for $\phi_{iso} > \phi_b$).[16–18,25,27] From the point at which the membrane touches the channel wall, r_{max} cannot increase further (Fig. 4a). The γ at $\phi_{iso} = \phi_b$ is the swelling ratio of buckling γ_b. For our membrane system, we found γ_b to be 1.042 ± 0.005 and ϕ_b = 0.968. With a Young's modulus of the used PDMS of E = 1.71 MPa (ref. 33) and its Poisson's ratio ν = 0.4950,[34] we obtain from eqn (2), a stress σ_b = (153 ± 18) kPa at the buckling point. Using the theory of elastic stability for thin plates, σ_b can be estimated by:[17]

$$\sigma_b = \frac{kE}{12(1-\nu^2)}\left(\frac{h_m}{b}\right)^2, \tag{3}$$

where k is the dimensionless buckling coefficient. k depends on the boundary conditions at the edges of the membrane, the shape of the membrane, and the stress distribution through the membrane, which makes it difficult to estimate a sufficient and precise theoretical value for our experimental case.[19,21,35]

By comparing σ and σ_b, we see that γ that causes the membrane to buckle is depending on the inverse of the aspect ratio by $\gamma - 1 \propto (b/h_m)^{-2}$. This dependence may provide potential access for controlled buckling of spatially selective parts or membranes in microfluidic devices at defined γ_b by adjusting the aspect ratio. While a membrane with $b/h_m = 10$ shows a buckling transition in our experiments, this is not the case for membranes with a lower aspect ratio (*e.g.*, for $b/h_m = 4$, ESI† S9).

Since γ_b does not depend on E (ref. 17 and 25) but on b/h_m, the buckling mechanism is possible for any type of material that can swell in response to its environment and has the required shape. Furthermore, γ_b can be varied by using different swelling solvents and solvent mixtures to swell the membranes, *e.g.*, binary isopropanol–ethanol mixtures (ESI† S10).

Impact of buckling membranes on flow resistance

To investigate the effect of buckling membranes on pressure-driven flows through the adjacent channels, we applied a pressure difference Δp of 0 hPa to 20 hPa between the in- and outlet of the microdevice. For these experiments, binary mixtures with ϕ_{iso} between 0.000 and 1.000 were flown trough the microdevice. The generated flow was low enough not to disturb the shape of the membrane and it maintained its overall shape for the range of Δp and ϕ_{iso} studied (ESI† S11). The resulting flow velocities vector field V were measured with particle imaging velocimetry (PIV)[30] from which a calculated flow rate $Q^* = vbh_c$ was determined using the average flow velocity v. The observed Q^* *versus* Δp at various ϕ_{iso} are displayed in Fig. 6a. For constant ϕ_{iso}, Q^* depends on Δp in a linear manner, as binary isopropanol–water mixtures behave like Newtonian fluids. With increasing ϕ_{iso}, a higher Δp is needed to cause a certain Q^*. The relation between Δp and Q^* is described by the slope which is the inverse of the hydraulic resistance $1/R(\phi_{iso})$

$$Q^* = \Delta p / R(\phi_{iso}). \tag{4}$$

To compare the effects of the buckling state of the membrane on pressure-driven flows, we corrected $R(\phi_{iso})$ for the fraction caused by pure swelling of the channel walls and normalized it to the viscosity of the mixtures,[36] resulting in the corrected hydraulic resistance $R^*(\phi_{iso})/\eta$ (ESI† S5).

The $R^*(\phi_{iso})/\eta$ dependence on ϕ_{iso}, depicted in Fig. 6b, can be separated into two distinct regions: for $\phi_{iso} < \phi_b$, it remains almost constant at an initial value of $R^*(\phi_{iso})/\eta$, and for $\phi_{iso} > \phi_b$, it increases rapidly with ϕ_{iso}. In the part of the channels passing the membrane, the heights of the channels h_c are changed by the membrane position as long as it does not remain in its centered, initial position. The channel heights are therefore described by $h_c = h_{c,0} \pm w_{n,m}$ with the initial channel heights $h_{c,0}$ (h_c at $\phi_{iso} = 0$). This results in an $n/2$-fold alternation of the channel heights with an amplitude of w_{max} in the buckling regime. The alternations decrease the

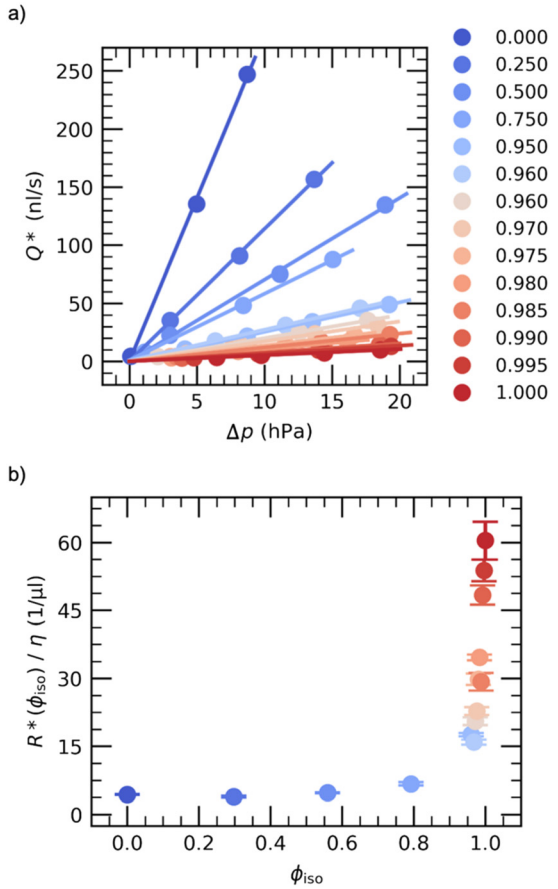

Fig. 6 a) Q^* of pressure-driven viscous flows through the channels caused by various pressure differences Δp. ϕ_{iso} of the measurements are marked with different colors (same color code for b), blue tones for $\phi_{iso} < \phi_b$ and red tones for $\phi_{iso} > \phi_b$. b) $R^*(\phi_{iso})/\eta$ for binary isopropanol–water mixtures with different ϕ_{iso} flowing through the channels.

hydraulic diameter $D_H = 4A/P$, with the channel cross section A, and the wetted perimeter P. Using D_H is a good approach in order to calculate the hydraulic resistance with $R^*(\phi_{iso})/\eta = 128l/(\pi D_H^4)$.[37] From this term, it becomes apparent that $R^*(\phi_{iso})/\eta$ increases with w_{max} even if the average channel cross sections averaged over the length a stay constant. The nonlinear dependence on D_H causes $R^*(\phi_{iso})/\eta$ to strongly increase for $\phi_{iso} > \phi_b$. In contrast, for a device with a membrane having a lower aspect ratio, no buckling can be observed, and $R^*(\phi_{iso})/\eta$ does not depend on ϕ_{iso}, as the membrane remains in the non-buckling regime with almost constant D_H for the full range of ϕ_{iso} (ESI† S5).

Since the resistance of rectangular channels is sensitive to the smallest dimension of the cross section h_c, it is critical to fabricate the microchannels and membranes in a well-defined fabrication process. Therefore, lithographic replica molding[28] is a suitable microfabrication method for the production of membrane-based resistors.

The characteristic time of swelling scales $t \propto h_m^2$,[38,39] resulting in a swelling time in the seconds range for the membrane. It is well known that the small size of at least one dimension of microfluidic structures overcomes the disadvantage of long swelling times in the microfluidic context.[40] Due to the chosen device design and the lamellar flow setup, shape transition times in the range of tens of seconds were observed after changing the solvent composition. No hysteretic effects were observed on these timescales, but this may be important in devices that can rapidly switch solvents or solvent compositions on timescales of seconds.

Thus, swelling-induced buckling of thin membranes is an effective mechanism for amplifying small swelling-induced changes that would not be sufficient to significantly affect fluid flows through the devices, *e.g.*, to alter volumetric flows by a large and abrupt change in hydraulic resistance $R(\phi_{iso})$ above a buckling volume fraction ϕ_b. This mechanism allows the manipulation of microfluidic channel geometries beyond what can be achieved by swelling alone. While conventional channels can only be adjusted to the extent of their absolute swelling,[40] channels with a height greater than the absolute swelling-induced change in size can be modified by deflecting the membrane through buckling.

Conclusions

We showed, how swelling-induced buckling of thin membranes can be used to change the channel geometry of microfluidic devices. The device we developed consists of a membrane embedded between two channels, which is highly sensitive to changes in the composition of the solvent mixtures flowing past. Depending on the swelling, the membrane can change its shape significantly due to swelling-induced buckling. The buckling pattern, characterized by an amplitude and a wavelength, depends on the ability of the solvents inside the microchannel to swell the membrane. The solvent-dependent large deflections of the membrane were used to modify the hydraulic resistance of the two microchannels. Due to the highly nonlinear swelling behavior of PDMS in isopropanol–water mixtures, a drastic change in hydraulic resistance could be achieved by changing the isopropanol volume fraction by $\Delta\phi_{iso} \lesssim 0.04$ with $\gamma_b \approx 1.04$. Since the critical swelling factor depends only on the geometry of the membrane and not on its mechanical properties, the buckling-based microresistor can be open to any type of material-stimuli system that allows the volume of the membrane to change. Due to this geometry-dependent buckling and thus the possibility to tailor the volume fraction of the buckling, one could imagine using these devices in microfluidic networks to selectively transport multicomponent solutions within the network depending on their composition.

Membrane-based resistors may be the starting point for more sophisticated manipulations of microfluidic flows. For example, the introduction of additional stimuli (*e.g.* pH,[41] temperature,[41,42] light,[43] glucose,[44] antigens,[45] electric fields,[46] magnetic fields[47]) or the interplay of different hydraulic parameters in the adjacent channels (*e.g.*, Q and Δp) would allow for more complex communication and

switching behavior. Furthermore, time-dependent manipulations can be introduced by a hysteresis of the membrane swelling. Even more complex interactions between the elastic behavior of the membranes and the hydrodynamic properties of the fluid flow in the adjacent channels can be introduced by implementing multiple membranes in the microdevices.

Author contributions

C.-H. S. and T. P. designed the research. C.-H. S., B. S. and F. L. performed the experiments. C.-H. S., B. S., F. L., E. M., and T. P. analyzed the data. C.-H. S. and T. P. wrote the paper with support of all authors.

Conflicts of interest

There are no conflicts to declare.

Acknowledgements

We would like to thank Brahim Bessif, Saba Telele and Günter Reiter for fruitful discussions. This work was funded by Deutsche Forschungsgemeinschaft under Grant No. PF375/6 within SPP 2171 and under Germany's Excellence Strategy – EXC-2193/1 – 390951807.

Notes and references

1 J. W. Hong, V. Studer, G. Hang, W. F. Anderson and S. R. Quake, *Nat. Biotechnol.*, 2004, **22**, 435–439.
2 T. Thorsen, S. J. Maerkl and S. R. Quake, *Science*, 2002, **298**, 580–584.
3 M. A. Unger, H. P. Chou, T. Thorsen, A. Scherer and S. R. Quake, *Science*, 2000, **288**, 113–116.
4 M. A. Gerspach, N. Mojarad, D. Sharma, T. Pfohl and Y. Ekinci, *Microsyst. Nanoeng.*, 2017, **3**, 17051.
5 M. A. Gerspach, N. Mojarad, D. Sharma, Y. Ekinci and T. Pfohl, *Part. Part. Syst. Charact.*, 2018, **35**, 1800161.
6 D. Sharma, R. Y. Lim, T. Pfohl and Y. Ekinci, *Microsyst. Nanoeng.*, 2021, **7**, 46.
7 T. Gervais, J. El-Ali, A. Günther and K. F. Jensen, *Lab Chip*, 2006, **6**, 500–507.
8 I. C. Christov, V. Cognet, T. C. Shidhore and H. A. Stone, *J. Fluid Mech.*, 2018, **841**, 267–286.
9 V. Iyer, A. Raj, R. K. Annabattula and A. K. Sen, *J. Micromech. Microeng.*, 2015, **25**, 75003.
10 M. Gomez, D. V. Moulton and D. Vella, *Phys. Rev. Lett.*, 2017, **119**, 144502.
11 D. P. Holmes, B. Tavakol, G. Froehlicher and H. A. Stone, *Soft Matter*, 2013, **9**, 7049–7053.
12 J. Kim, J. A. Hanna, M. Byun, C. D. Santangelo and R. C. Hayward, *Science*, 2012, **335**, 1201–1205.
13 J.-H. Na, N. P. Bende, J. Bae, C. D. Santangelo and R. C. Hayward, *Soft Matter*, 2016, **12**, 4985–4990.
14 L. Huang, R. Jiang, J. Wu, J. Song, H. Bai, B. Li, Q. Zhao and T. Xie, *Adv. Mater.*, 2017, **29**, 1605390.
15 T. Mora and A. Boudaoud, *Eur. Phys. J. E: Soft Matter Biol. Phys.*, 2006, **20**, 119–124.
16 Z. Liu, W. Hong, Z. Suo, S. Swaddiwudhipong and Y. Zhang, *Comput. Mater. Sci.*, 2010, **49**, 60–64.
17 S. P. Timošenko and J. M. Gere, *Theory of Elastic Stability*, McGraw-Hill Book, New York, USA, 1961.
18 S. P. Timošenko and S. Woinowsky-Krieger, *Theory of plates and shells*, McGraw-Hill Book, New York, USA, 1976.
19 J. Betten and C. H. Shin, *Forsch. Ingenieurwes.*, 2000, **65**, 273–278.
20 A. Moslemi, B. Navayi Neya and J. Vaseghi Amiri, *Appl. Math. Model.*, 2016, **40**, 5717–5730.
21 W. H. Wittrick, *Aeronautical Quarterly*, 1954, **4**, 83–92.
22 C. Yu and B. W. Schafer, *J. Eng. Mech.*, 2007, **133**, 452–463.
23 Y. Xiong and O. Kuksenok, *Langmuir*, 2021, **37**, 4900–4912.
24 W. Hong, Z. Liu and Z. Suo, *Int. J. Solids Struct.*, 2009, **46**, 3282–3289.
25 R. Jiang, J. Xiao and J. Song, *Theor. Appl. Mech. Lett.*, 2017, **7**, 134–137.
26 E. Sharon and E. Efrati, *Soft Matter*, 2010, **6**, 5693.
27 J. Gemmer and S. C. Venkataramani, *Soft Matter*, 2013, **9**, 8151.
28 Y. Xia and G. M. Whitesides, *Annu. Rev. Mater. Sci.*, 1998, **28**, 153–184.
29 J. Schindelin, I. Arganda-Carreras, E. Frise, V. Kaynig, M. Longair, T. Pietzsch, S. Preibisch, C. Rueden, S. Saalfeld, B. Schmid, J.-Y. Tinevez, D. J. White, V. Hartenstein, K. Eliceiri, P. Tomancak and A. Cardona, *Nat. Methods*, 2012, **9**, 676–682.
30 W. Thielicke and R. Sonntag, *J. Open Res. Softw.*, 2021, **9**, 12.
31 M. H. Sadd, *Elasticity. Theory, Applications, and Numerics*, Elsevier, USA, Burlington, 2009.
32 B. Audoly and A. Boudaoud, *Phys. Rev. Lett.*, 2003, **91**, 86105.
33 I. D. Johnston, D. K. McCluskey, C. K. L. Tan and M. C. Tracey, *J. Micromech. Microeng.*, 2014, **24**, 35017.
34 A. Müller, M. C. Wapler and U. Wallrabe, *Soft Matter*, 2019, **15**, 779–784.
35 E. C. Oba, P. C. Anyadiegwu, A. G. T. George and E. C. Nwadike, *International Journal of Scientific and Research Publications*, 2018, **8**, 2250–3153.
36 F.-M. Pang, C.-E. Seng, T.-T. Teng and M. H. Ibrahim, *J. Mol. Liq.*, 2007, **136**, 71–78.
37 F. M. White, *Fluid Mechanics*, McGraw-Hill, New York, 2011.
38 T. Tanaka, *Phys. A*, 1986, **140**, 261–268.
39 T. Tanaka and D. J. Fillmore, *J. Chem. Phys.*, 1979, **70**, 1214–1218.
40 D. J. Beebe, J. S. Moore, J. M. Bauer, Q. Yu, R. H. Liu, C. Devadoss and B.-H. Jo, *Nature*, 2000, **404**, 588–590.
41 T. Tanaka, D. Fillmore, S.-T. Sun, I. Nishio, G. Swislow and A. Shah, *Phys. Rev. Lett.*, 1980, **45**, 1636–1639.
42 J. Hoffmann, M. Plötner, D. Kuckling and W.-J. Fischer, *Sens. Actuators, A*, 1999, **77**, 139–144.
43 A. Suzuki and T. Tanaka, *Nature*, 1990, **346**, 345–347.
44 K. Kataoka, H. Miyazaki, M. Bunya, T. Okano and Y. Sakurai, *J. Am. Chem. Soc.*, 1998, **120**(48), 12694–12695.
45 T. Miyata, N. Asami and T. Uragami, *Nature*, 1999, **399**, 766–769.

46 T. Tanaka, I. Nishio, S.-T. Sun and S. Ueno-Nishio, *Science*, 1982, **218**, 467–469.

47 N. Kato, S. Yamanobe and F. Takahashi, *Mater. Sci. Eng., C*, 1997, **5**, 141–147.